Chemistry–A European Journal
Research Article
doi.org/10.1002/chem.202302093
Chemistry Europe
European Chemical Societies Publishing
www.chemeurj.org

An Artificial Liposome Compartment with Size Exclusion Molecular Transport

Shiwei Zhang,[a] Eiji Nakata,[a] Peng Lin,[a] and Takashi Morii*[a]

The cellular compartment plays an essential role in organizing the complex and diverse biochemical reactions within the cell. By mimicking the function of such cellular compartments, the challenge of constructing artificial compartments has been taken up to develop new biochemical tools for efficient material production and diagnostics. The important features required for the artificial compartment are that it isolates the interior from the external environment and is further functionalized to control the transport of target chemicals to regulate the interior concentration of both substrate and reaction products. In this study, an artificial compartment with size-selective molecular transport function was constructed by using a DNA origami-guided liposome prepared by modifying the method reported by Perrault et al. This completely isolates the liposome interior, including the DNA origami skeleton, from the external environment and allows the assembly of a defined number of molecules of interest inside and/or outside the compartment. By incorporating a bacterial membrane protein, OmpF, into the liposome, the resulting artificial compartment was shown to transport only the molecule of interest with a molecular weight below 600 Da from the external environment into the interior of the compartment.

Introduction

Among the complex and diverse metabolic reactions within the cell, certain types of enzymes are highly organized and distributed on specific protein scaffolds or compartment membranes to achieve better control over biological processes.[1,2] The benefits of such an organized system include the avoidance of cross-inhibition and other incompatibilities that can occur in complex cascade reactions.[3,4] The regulation of proton and substrate fluxes across the lipid membrane of these compartments is critical and is mediated by membrane proteins that play a central role in maintaining cytoplasmic and extracellular pH balance and facilitating the co-transport of metabolites and ions.[5] Artificial compartments have the potential to mimic the cellular compartments[6] and have a wide range of applications, including biosensing,[7] drug delivery,[8] and bioreactors.[9] These compartments can be constructed using a variety of materials, including liposomes,[10] protein cages,[11] DNA origami cages,[12] and inorganic nanoparticles.[13] The important features required for the artificial compartment to mimic the cellular compartment are that its interior is isolated from the external environment and that it provides a scaffold for organizing the molecules of interest on and/or within the compartment. This is because living cells have highly compartmentalized organelles that optimize reactions and activities by occupying independent spaces or locations isolated from the external environment. Another important property of artificial compartments is the ability to control the transport of substances of interest, which is achieved by incorporating membrane proteins, transporters, and channels, such as AqpZ,[14] OmpF,[15] and FhuA[16] for bacteria, into phospholipid membranes. These components allow the transport of molecules and ions of interest, such as substrates and reaction products, while selectively filtering them based on their intrinsic properties. The advancement of artificial compartments not only deepens our understanding of cellular metabolism but also expands their potential for a wide range of applications, including chemical synthesis, sensing, and functional biomaterials. However, the construction of an artificial compartment that can simultaneously organize molecules of interest in the interior space and locate membrane proteins remains a challenge.

With the development of DNA nanotechnology, addressable DNA nanostructures provide ideal platforms with various sizes and shapes[17] for the assembly of dyes,[18,19] nanoparticles,[20,21] multiple proteins,[22,23] allowing the construction of a variety of enzyme assemblies and enzyme cascades.[24–27] At the same time, rationally designed DNA nanostructures were modified with lipid molecules at controlled positions to promote the formation of liposomes of defined size.[28] DNA nanostructures have served as high-precision templates for membrane engineering and have provided a promising route for the construction of confined membrane structures.[29–32]

In this study, an artificial liposome compartment with a uniform diameter of ~80 nm was constructed using an internal DNA origami skeleton prepared by modifying the design reported by Perrault et al.[33] to realize the following features: its interior is isolated from the external environment and it provides a scaffold for organizing the molecules of interest. The

[a] S. Zhang, Prof. E. Nakata, Dr. P. Lin, Prof. T. Morii
Institute of Advanced Energy, Kyoto University
Uji, Kyoto, 6110011 (Japan)
E-mail: t-morii@iae.kyoto-u.ac.jp

Supporting information for this article is available on the WWW under https://doi.org/10.1002/chem.202302093

internal DNA origami skeleton was modified with a defined number of pH-sensitive and/or pH-insensitive fluorophores to monitor pH changes around the skeleton. The pH-sensitive fluorophore attached to a naked DNA origami skeleton to protrude inside the skeleton responded to changes in buffer pH, whereas the emission did not respond to pH changes when the skeleton was encapsulated by liposome. This indicates that the internal DNA origami skeleton has been successfully isolated from the external environment by liposome encapsulation. The artificial compartment prepared in this way was further functionalized with a size exclusion molecular transport function by incorporating a natural transporter. A bacterial membrane protein, OmpF, enables the direct transport of small molecules with molecular weights below 600 Da.[34] When OmpF was incorporated into the liposome compartment, the emission of the pH-sensitive fluorophore on the internal DNA origami skeleton of the artificial compartment responded to the pH change of the external buffer. Finally, the size exclusion transport of OmpF was evaluated by adding an intercalator to the external buffer. The OmpF-incorporated compartment allowed an intercalator with a molecular weight below 600 Da to bind to the internal DNA skeleton, whereas the OmpF-embedded compartment prevented an intercalator with a molecular weight above 600 Da from binding to the DNA skeleton. This indicates that OmpF has been successfully incorporated into the membrane in an active form. The artificial compartment with the membrane protein has the potential to control the transport of small molecules through the membrane protein located on the membrane assembled DNA origami skeleton and to selectively exchange small molecules of interest including substrate and product of the cascade reaction constructed in the internal environment.

Results and Discussion

Design of wireframe DNA origami as the internal skeleton for the artificial compartment

To construct the artificial compartment, a wireframe DNA origami skeleton (WS) that was modified from the design of Perrault et al.[33] to allow the assembly of fluorophores of interest at defined locations, was used as the inner skeleton of a liposome compartment (Figure 1a). The three-dimensional (3D) structure of the WS consisted of 12 frames, each consisting of a bundle of six double helices of approximately 50 nm diameter. These frames serve as a scaffold for the assembly of fluorophores and lipid.

A set of 48 identical handles (comp-ODN-tag1) protruding from the outer side of the frames was designed for the attachment of lipidated ODN (lipidated ODN-tag1) (Figure S1). Two sets of 12 identical handles with orthogonal nucleotide sequences (comp-ODN-tag2 and comp-ODN-tag3), protruding from the inner surface of the frames of WS, were designed to allow the attachment of two types of fluorophores, 12 molecules each, modified with the specific short single-stranded

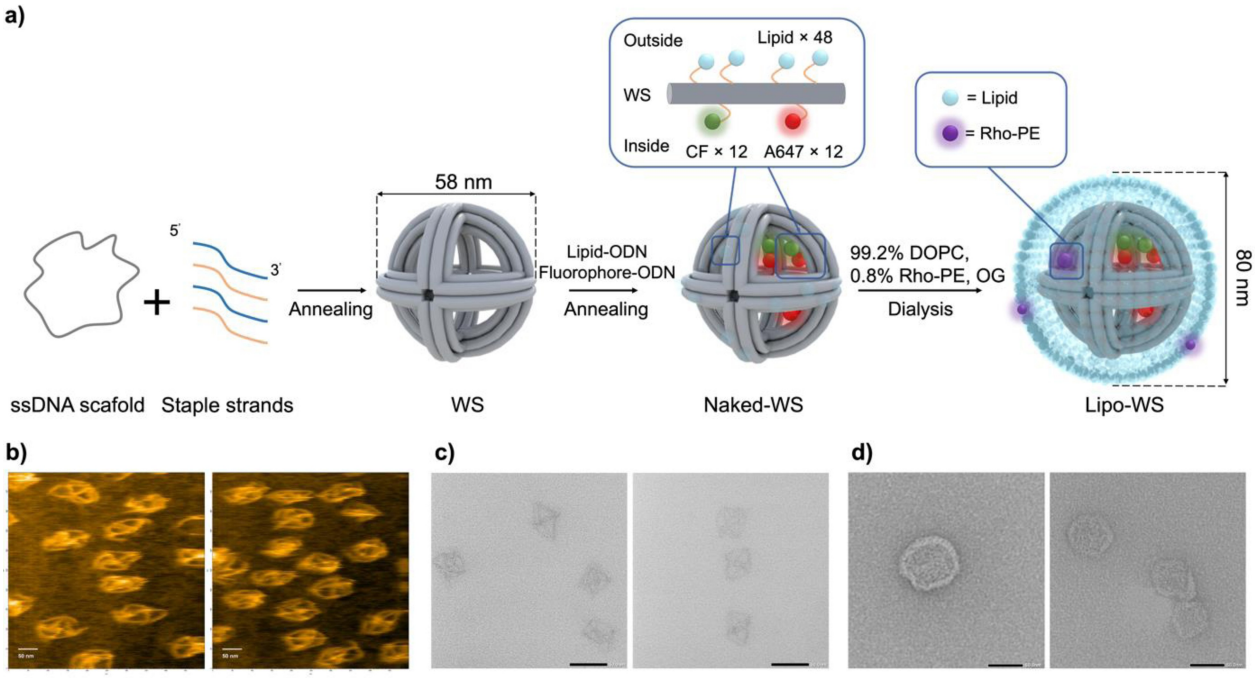

Figure 1. (a) Scheme illustrating the construction of an artificial compartment. A DNA origami skeleton (WS) was assembled with multiple fluorophores, 6-carboxyfluorescein (CF) and Alexa 647 (A647), using a CF-modified ODN-tag and an A647-modified ODN-tag, respectively, and with a lipid modified ODN-tag (lipidated ODN). The sequence information of fluorophore or lipid modified ODN-tag and their complementary sequences of them are shown in Figure S1 in the Supporting Information. The lipidated ODN was attached to the outer handles of the DNA origami skeleton (naked-WS) in a surfactant solution, which formed mixed surfactant-lipid micelles around the lipidated ODN-tag to form liposomes. The surfactant was removed by dialysis to form a fused lipid bilayer around the DNA origami skeleton (lipo-WS). (b) AFM images of purified WS. Scale bar: 50 nm. (c) TEM images of purified WS. Scale bar: 50 nm. (d) TEM images of lipo-WS. Scale bar: 50 nm.

DNA (ODN-tag2 and ODN-tag3), by specific hybridization to WS (Figure S1).

A scaffold DNA (p7308) was folded with 144 short single-stranded DNA (Table S5) into WS as a programmable shape by a thermal annealing step for 15 h. The folded WS was purified with Sephacryl S-400 to remove excess staple strands (Figure S2) and characterized by atomic force microscopy (AFM) (Figure 1b) and transmission electron microscopy (TEM) (Figure 1c). The diameter of WS was determined to be 59.3 ± 6.5 nm and 58.6 ± 5.5 nm in the AFM and TEM images, respectively, which were consistent with the designed sizes (Figure S3 and S4).

Construction of the artificial compartment guided by a wireframe DNA origami skeleton

A pH sensitive fluorophore 6-carboxyfluorescein (CF) with a pK_a of 6.5[35] and a pH insensitive fluorophore Alexa 647 (A647) were chosen to assemble the inner side of the WS for ratiometric pH monitoring (Figure 1a). A647 modified ODN-tag2 (A647-ODN) and CF modified ODN-tag3 (CF-ODN) were used to hybridize with complementary sequences of them located inside the WS (comp-ODN-tag2 and comp-ODN-tag3). Lipidated ODN conjugated with thiol-modified ODN-tag1 and DOPE-MAL (see Figure S5),[36] was hybridized in the presence of *N*-octyl-β-D-glucoside (OG) to the outer set of 48 handles protruding from the outer surface of the WS to promote tight wrapping of the membrane around the structure. The modified DNA origami skeleton (naked-WS, Figure 1a) was subsequently mixed with DOPC containing 0.8% rhodamine modified lipid (1,2-dioleoyl-sn-glycero-3-phosphoethanolamine-N-(lissamine rhodamine B sulfonyl) ammonium salt, Rho-PE) in a solution containing OG at its critical micelle formation concentration (CMC) (0.67% (w/v)).[37] The lipid bilayer was reconstituted by a dialysis step. The dialyzed solution was loaded onto an iodixanol gradient, optimized based on our previous work[32] to maximize recovery yield, and spun in an ultracentrifuge to separate liposome-coated WS (lipo-WS) (Figure S6a).

The separated fractions were characterized by agarose gel electrophoresis analysis. WS lacking the lipidated ODN was also prepared and fractionated for comparison (Figure 2). Fractions collected after ultracentrifugation were loaded onto an agarose gel containing 0.05% SDS to disrupt the liposome. Fluorescence emissions from A647 and Rho were measured as the indication of WS and liposome, respectively. In the case of the lipo-WS (Figure 2, right), the initial fractions (F1-4) showed only one band with the fluorescence of Rho, indicating that these fractions contained only the lipid. In the subsequent fractions (F5-7), both a band corresponding to WS and a band corresponding to liposomes were observed, indicating the presence of lipo-WS. The denser fractions (F8-11) showed the bands corresponding to the excess of A647-ODN. In contrast, the band corresponding to WS appeared mainly in the denser fractions (F8-11) and the band corresponding to lipids appeared mainly in the initial fractions (F1-4) in the case of WS without the lipidated ODN (Figure 2, left). Without the modification of

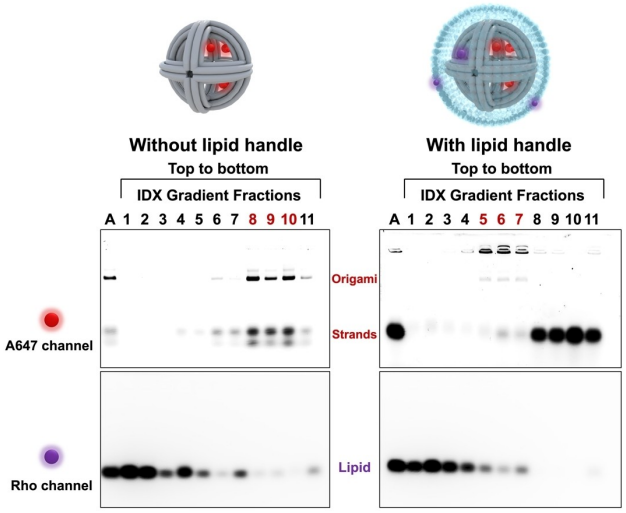

Figure 2. Agarose gel images of the density gradient fractions of WS without lipid handle (left) or with lipid handle (right). Fractions are numbered sequentially from F1 to F11 from the top to the bottom of the gradient as shown in Figure S6. Lane A: before purification.

WS by lipidated ODN, WS and lipid did not coexist in the same fraction. These results indicated the specific formation of lipo-WS in fractions (F5-7). The separated fraction containing lipo-WS was analyzed by TEM (Figure 1d and Figure S6b). The outer membrane diameter of lipo-WS was determined by TEM images to be 79.6 ± 9.1 nm (Figure S6c), consistent with the designed size (Figure 1a).

Characterization of the artificial compartment by fluorescence microscopy

The successful construction of artificial compartments was independently verified by colocalizing the fluorescence signal of A647- and CF-modified WS with Rho-PE-containing liposomes (lipo-WS). To immobilize lipo-WS on a microscope slide, the lipo-WS was modified with biotin-PE (1-oleoyl-2-(12-biotinyl(aminododecanoyl))-sn-glycero-3-phosphoethanolamine) (Figure 3a). As a control, liposomes containing Rho-PE and biotin-PE (lipo), and a naked DNA origami skeleton (naked-WS) carrying A647 and CF modified with biotinylated ODN were also prepared (see Materials and Methods). They were then immobilized on a biotin-BSA coated microscope slide modified with a streptavidin using a biotin/streptavidin interaction (see Figure 3a and Materials and Methods). Under microscopic observation, the fluorescence emission of CF, Rho, and A647 almost coexisted at the same position in the fluorescence image of lipo-WS. Based on the correlation analysis, the channel of A647 and Rho showed a strong positive correlation with a Pearson's correlation coefficient of 0.84 (Figure S7).[38] On the other hand, in the case of lipo and naked-WS, respectively, the fluorescence emission of only Rho or that of only CF and A647 was observed. The result indicated the successful construction of lipo-WS in a near quantitative yield.

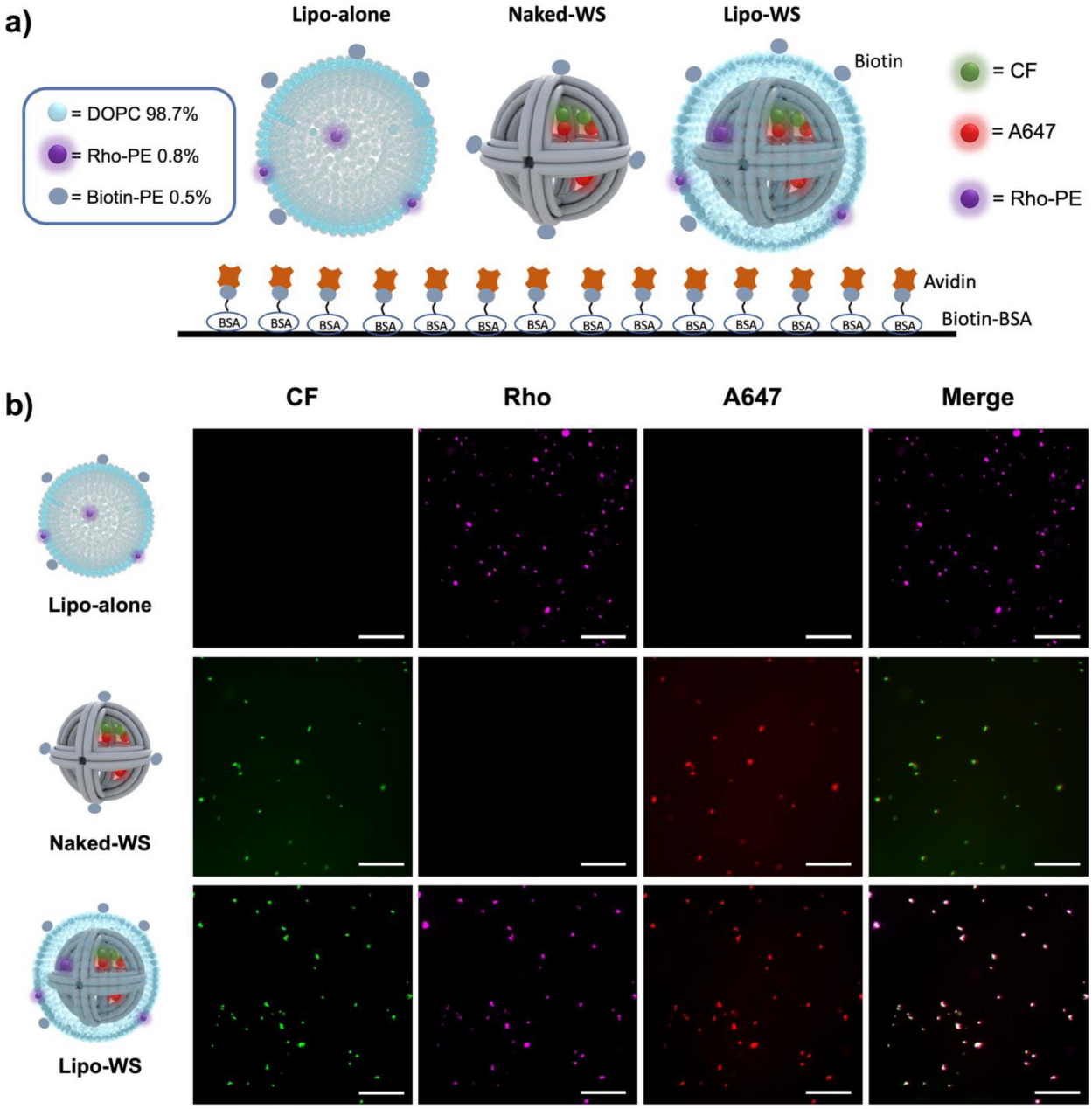

Figure 3. (a) Illustration showing the immobilized lipo-WS. Liposomes are formulated with fluorophore-labelled lipids, Rho-PE (Rho). WS are modified with CF and A647 and immobilized on a biotin-BSA and streptavidin-coated surface using a biotin-streptavidin interaction. (b) Fluorescence image of liposome, naked-WS and lipo-WS after surface immobilization in CF channel, Rho channel and A647 channel. Scale bar: 100 μm.

The encapsulation of WS by liposome as an artificial compartment was verified by taking advantage of the sensitivity of CF emission to pH changes.[35] The pH titration of naked-WS was performed in a test tube (Figure S8) and the plot gave an estimate of the pK_a of CF on naked-WS (7.3 ± 0.2). The estimated pK_a value was shifted to the basic side compared to free CF (pK_a = 6.5) due to the destabilization of the dianionic form of CF by the negative charge of the DNA phosphate backbone of WS, which is consistent with that of CF on a DNA nanostructure as reported previously.[32,39] The result indicated that the fluorescence emission of CF on naked-WS retained its sensitivity to pH changes and was effectively decreased at pH 6.0. Fluorescence microscopy analyses of naked-WS were carried out by changing the pH of the outer buffer (Figure 4a and S9). First, the immobilized naked-WS, of which the CF fluorophores assembled on the inner side of the frame were exposed to the bulk solution, was analyzed at pH 8.0. In this case, CF showed strong fluorescence (Figure S9, top column). When the buffer was changed to pH 6.0, the fluorescence of CF was drastically reduced to 35 ± 7% of the initial fluorescent intensity (Figure S9, middle column). By changing the buffer back to pH 8.0, the reduced fluorescence of CF at pH 6.0 was restored to almost the same fluorescence intensity as the initial fluorescence at pH 8.0 (Figure S9, bottom column, and Ta-

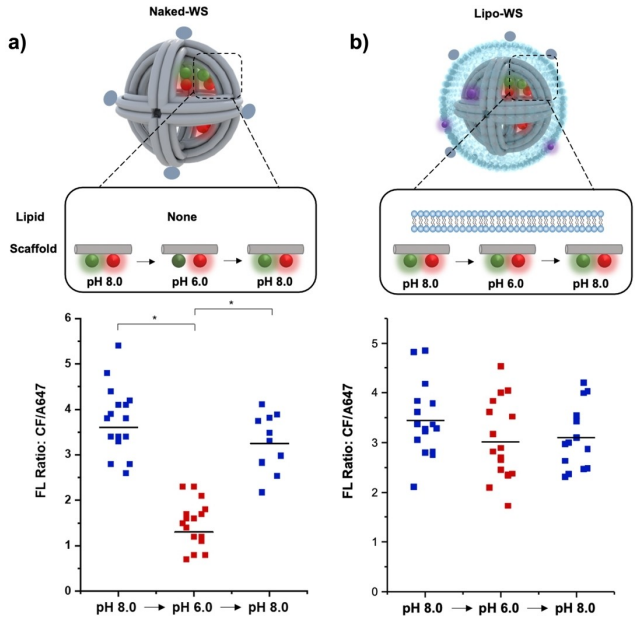

Figure 4. Plot of fluorescence intensity ratio (CF/A647) of individual naked-WS (a) and lipo-WS (b) in each indicated pH condition. Asterisks indicate significant difference between groups (*$p < 0.001$). The fluorescence image and the raw data are shown in Figure S10–11 and Table S1–S2, respectively.

ble S1). On the other hand, the fluorescence of A647 showed constant fluorescence during these pH changes. The fluorescence of CF on the naked-WS responded well to the pH change of the bulk buffer solution with the constant fluorescence of A647 as the internal standard. The ratio of CF/A647 of individual spots derived from naked-WS was plotted in Figure 4a, and the ratio of CF/A647 between pH 8.0 and pH 6.0, and pH 6.0 and pH 8.0 showed a significant difference. In contrast, the fluorescence intensity of CF of lipo-WS showed no significant difference during the sequential change of the outer buffer from pH 8.0 to pH 6.0 and then back to pH 8.0, maintaining almost 100% of the initial fluorescence intensity (Figure S10 and Table S2). The plot of the ratio of CF/A647 of single spots derived from lipo-WS during the pH change of the outer buffer showed no significance (Figure 4b). These results strongly indicated that the WS of lipo-WS was well encapsulated inside the liposome and sealed from the external pH variation, and demonstrated that lipo-WS possessed the key features of an artificial compartment.

Construction and characterization of an artificial compartment incorporating a bacterial membrane protein OmpF

After formation and purification of the artificial compartment lipo-WS, different concentrations of purified OmpF were mixed with lipo-WS and incubated at 37 °C for 1 h to insert OmpF into the membrane (Figure 5a, see Materials and Methods for details). The amount of OmpF loaded on lipo-WS was estimated by SDS-PAGE analysis of the purified OmpF-embedded lipo-WS (lipo-OmpF-WS, see Figure S12, Table S3, and Materials and Methods). When 100 nM to 4000 nM OmpF was incubated with the constant amount of lipo-WS, an average of 2.9 to 3.6 trimers were incorporated per lipo-OmpF-WS. OmpF or its trimer was reconstituted into the liposomes of lipo-OmpF-WS without controlling the orientation. Incorporation of OmpF into lipo-WS caused little or no perturbation of the parent lipo-WS structure in the TEM images (Figure S13). Based on this observation, the lipo-WS compartment (4 nM) was incubated with OmpF (1000 nM) and purified to yield lipo-OmpF-WS with an average of 3.0 trimers per compartment, which was used for further experiments.

The lipo-OmpF-WS compartment was immobilized on a microscope slide as described in the previous section (Figure 3a). Strong spots of fluorescence emission from the CF fluorophore in lipo-OmpF-WS were observed at pH 8.0 (Figure 5b, Figure S14 and Table S4), as did naked-WS and lipo-WS (Figure 4). When the external buffer was changed from pH 8.0 to pH 6.0, the fluorescence intensity of CF inside the OmpF-embedded lipo-OmpF-WS dramatically decreased to 35 ± 5% of the initial fluorescence intensity, which was similar to the case of naked-WS (Figure 4a). This is in sharp contrast to the result obtained with lipo-WS without OmpF, where the fluorescence of the CF in lipo-WS was not significantly altered (Figure 4b). The reduced fluorescence of CF in lipo-OmpF-WS was restored to 92 ± 7% of the initial fluorescence when the external buffer was changed back to pH 8.0. These observations were consistent with the expected function for lipo-OmpF-WS (Figure 5c). The ratio of CF/A647 of individual spots derived from lipo-OmpF-WS was plotted (Figure 5c), and the CF/A647 between pH 8.0 and pH 6.0, and pH 6.0 and pH 8.0 again showed a significant difference. It should be noted that all individual lipo-OmpF-WS spots in the ratio of CF/A647 responded significantly to the pH change, indicating that OmpF was uniformly incorporated into each of the lipo-WS with activity maintained. These results indicate that the membrane protein OmpF was successfully reconstituted into the liposome of the lipo-OmpF-WS artificial compartment in an active form, thus allowing the buffer to permeate through the lipo-OmpF-WS membrane.

Size-dependent permeation of small molecules through an OmpF-embedded artificial compartment

The size-dependent transport of OmpF embedded in the artificial compartment was evaluated using two different sizes of intercalators (Figure S15), EtBr (molecular weight: 394.3) and a bis-intercalator GelRed (molecular weight: 1239.1), both of which increase the fluorescence intensity upon binding to DNA, in this case the DNA origami skeleton WS. Naked-WS, lipo-WS, and lipo-OmpF-WS were modified with A647 and biotin, immobilized, and then analyzed by fluorescence microscopy. In all cases, bright spots corresponding to the fluorescence of A647 in WS were observed. When EtBr or GelRed was added to the buffer containing naked-WS, the strong fluorescence of EtBr or GelRed was colocalized with the fluorescence of A647. Changes in the ratio of EtBr/A647 or GelRed/A647 of individual spots derived from naked-WS showed a significant increase as

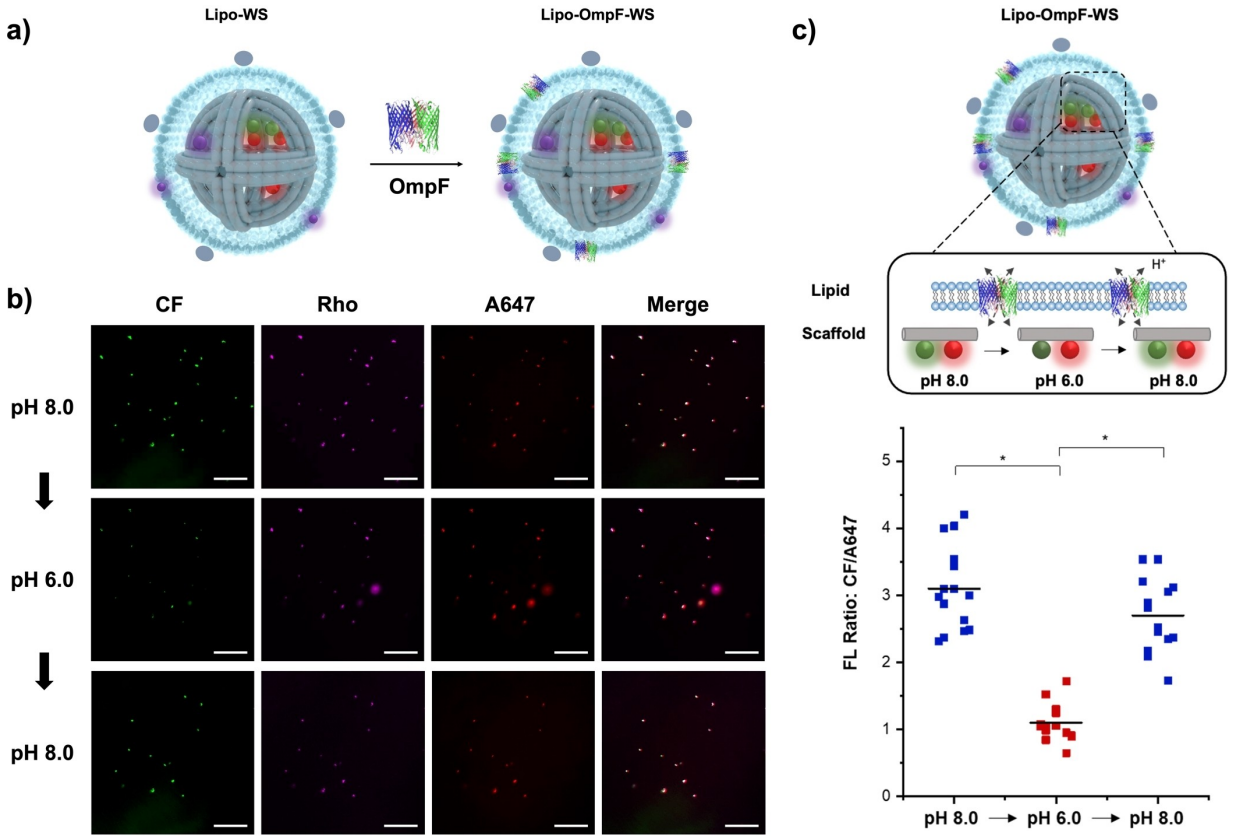

Figure 5. (a) Schematic illustration of the insertion of OmpF into the membrane of lipo-WS (lipo-OmpF-WS) to construct an artificial compartment with a transporter. (b) Fluorescence images of lipo-OmpF-WS after immobilization on a biotin-BSA and streptavidin-coated surface acquired at the CF channel, Rho channel and A647 channel at pH 8.0 and 6.0, respectively. Scale bar: 100 μm. (c) Illustration of buffer diffusion through the OmpF-embedded membrane of lipo-OmpF-WS. Plot of fluorescence intensity ratio (CF/A647) of individual lipo-OmpF-WS in each pH condition (pH 8.0, pH 6.0 and pH 8.0 again). Asterisks indicate significant difference between groups (***p* < 0.001).

shown in Figure 6a and Figure S16. These results indicate that both intercalators avidly bind to naked-WS. On the other hand, the fluorescence of EtBr and GelRed was not increased in the case of lipo-WS, and the plot of the ratio of EtBr/A647 or GelRed/A647 of lipo-WS showed no significant difference before and after the addition of intercalators (Figure 6b and Figure S17). The WS DNA skeleton in lipo-WS was well shielded within the liposome, which completely prevented the binding of the intercalators to WS DNA. The lipo-OmpF-WS showed a different behavior with the addition of either EtBr or GelRed. Upon addition of EtBr, the fluorescence emission of EtBr colocalized with the A647 emission spots of lipo-OmpF-WS, but the addition of GelRed showed no additional emission to the A647 emission spots (Figure 6c and Figure S18). The plot of the EtBr/A647 ratio of lipo-OmpF-WS showed a significant increase, but that of GelRed/A647 showed no difference. The OmpF-embedded compartment lipo-OmpF-WS allowed the binding of EtBr, which has a molecular weight lower than 600 Da, to the internal DNA skeleton WS but prevented the binding of GelRed, which has a molecular weight higher than 600 Da. The same trends were observed by monitoring the fluorescence intensity of the bulk solution as follows: A solution containing naked-WS, lipo-WS, or lipo-OmpF-WS, was incubated with EtBr or GelRed, and then treated SDS was added to disrupt the liposome (Figure 6d-4f). When naked-WS was incubated with EtBr or GelRed, the fluorescence derived from the intercalator increased rapidly in both cases, indicating that both EtBr and GelRed bound to WS (Figure 6d). Incubation of lipo-WS with EtBr or GelRed failed to increase the fluorescence relative to the background, indicating that neither was able to bind the WS in lipo-WS. In both cases, EtBr and GelRed, when SDS was added to the mixture of lipo-WS and the intercalator, the fluorescence increased rapidly (Figure 6e). This indicates that the addition of SDS disrupts the membrane to expose WS to the bulk solution, which promotes the binding of intercalators to WS. In the case of lipo-OmpF-WS, the fluorescence of EtBr increased rapidly, but that of GelRed did not (Figure 6e). When SDS was added, the fluorescence of EtBr showed no obvious change, but that of GelRed increased rapidly. The OmpF on lipo-OmpF-WS effectively allows EtBr to diffuse from the external buffer into the liposome, but prevents the transport of GelRed, demonstrating the inherent size exclusion of molecules with a molecular weight of 600 Da. These results support the fact that OmpF has been successfully incorporated into the membrane of lipo-OmpF-WS in an active form to functionalize the artificial compartment.

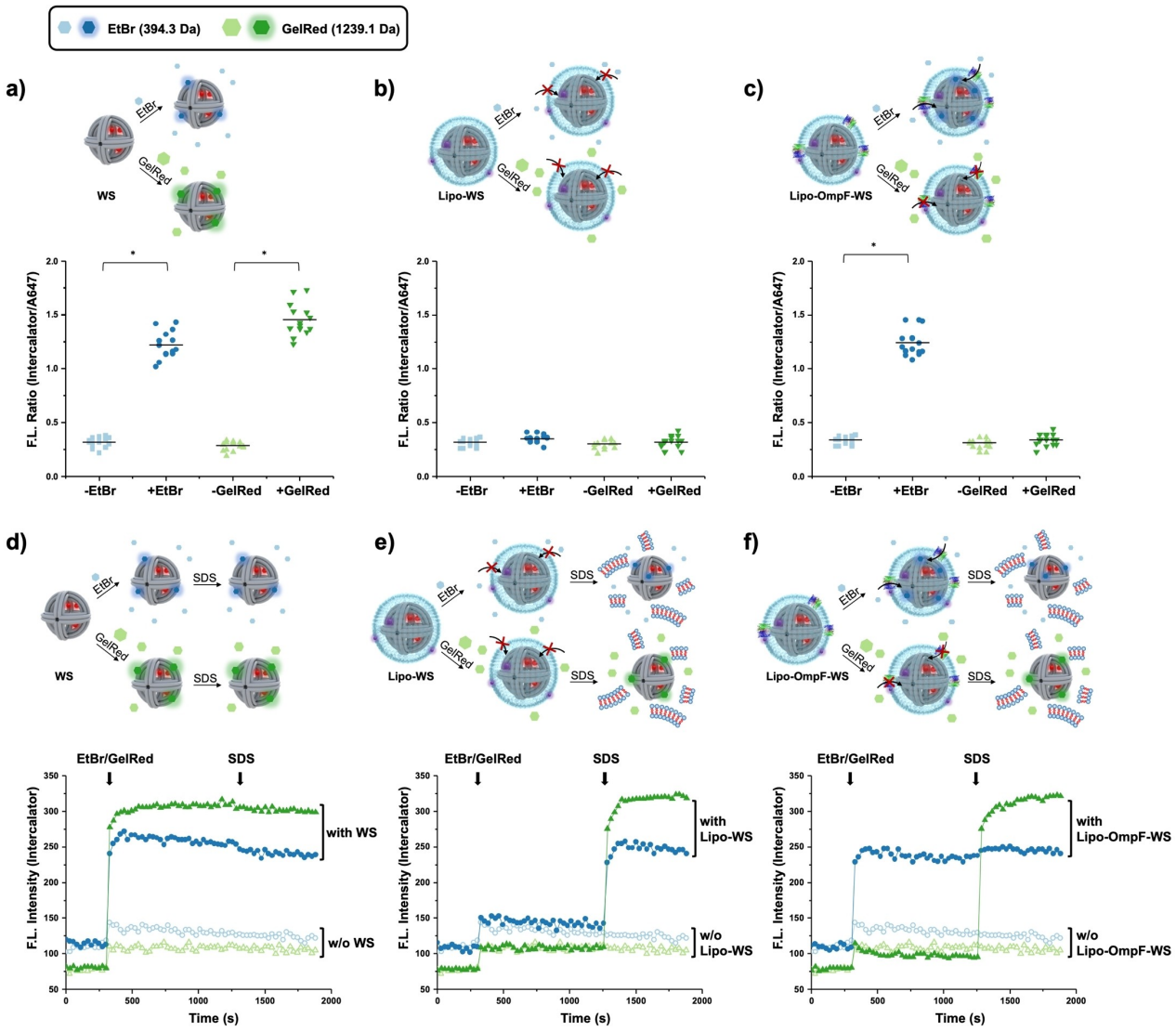

Figure 6. (a-c) Plot of fluorescence intensity ratio (intercalator/A647) of individual (a) naked-WS, (b) lipo-WS or (c) lipo-OmpF-WS with and without intercalators (blue: EtBr; green: GelRed). Asterisks indicate significant differences between groups (*$p < 0.001$). Their fluorescence images are shown in Figures S15–17. (d-f) The changes in fluorescence intensity of intercalators when mixed with (d) naked-WS, (e) lipo-WS, or (f) lipo-OmpF-WS and followed by addition of SDS. Control experiments were performed with intercalators without WS derivatives. Fluorescence intensity was monitored in a 96-well microplate. Filled circles: EtBr with WS derivatives, filled triangles: GelRed with WS derivatives, empty circles: EtBr without WS derivatives, empty triangles: GelRed without WS derivatives.

Conclusions

The artificial compartment was constructed by a wireframe DNA origami skeleton (WS), which provided a platform for the introduction of molecules of interest encapsulated by liposomes. The formation of the DNA origami skeleton was characterized by means of agarose gel electrophoresis, AFM and TEM measurements. The encapsulation of the DNA origami skeleton by liposomes (lipo-WS) was confirmed by monitoring the pH change of the internal space of the compartment, which was well sealed from the external buffer. It should be noted that almost all the lipo-WS isolated by ultracentrifugation were well sealed and could act as an artificial compartment.

By incorporating the membrane protein OmpF into the lipid bilayer of the liposome, the active OmpF successfully altered the internal pH of the compartment. As shown in this study, OmpF allows the direct passage of not only protons, but also small molecules with a molecular weight of less than 600 Da.[40] This means that we have successfully constructed an artificial compartment that can not only be isolated from the external environment, but can also control the transport of specific chemicals across the membrane. The DNA origami skeleton can also be used as a platform to locate proteins and enzymes of interest using the modular adaptors developed by our group.[41–43] Our laboratory is currently developing a method to place a defined number of enzymes and membrane proteins on the DNA origami skeleton to construct a cascade reaction within the artificial compartment.

Experimental Section

Materials: Purified oligonucleotide as the staple strands for DNA origami and all other oligonucleotides were purchased from Sigma-Aldrich (St. Louis, MO, USA) or Thermo Fisher Scientific Inc. Ultrafree-MC–DV and Amicon Ultra-0.5 mL Centrifugal Filters were purchased from Merck Millipore (Darmstadt, Germany). Lissamine™ rhodamine B DHPE, triethylammonium salt (Rho-PE), biotinylated bovine serum albumin and NeutrAvidin were purchased from Thermo Fisher Scientific Inc. (Waltham, MA, USA). 1,2-Dioleoyl-sn-glycero-3-phosphocholine (DOPC) was purchased from Sigma-Aldrich (St. Louis, MO, USA). Dioleoyl-sn-glycero-3-phosphoethanolamine-N-(maleimidomethyl) (DOPE-MAL) was purchased from NOF CORPORATION (Tokyo, Japan). *N*-Octyl-β-D-glucoside (OG) was purchased from DOJINDO (Kumamoto, Japan). Opti Prep (60% iodixanol solution) was purchased from Axis-Shield Diagnostics Ltd. (Dundee, England). TI blue was purchased from Nissin EM Co., Ltd. (Tokyo, Japan). 15 nm carbon grid U1017 from EM Japan (Tokyo, Japan) was used for the TEM grid. μ-Slide I0.2 Luer ibidi Treat was purchased from ibidi (Gräfelfing, Germany). Low-binding microtube (BT-150 L, 1.5 mL, nonpyrogenic & RNase- / DNase- free) was purchased from Ina OPTIKA CO., LTD (Osaka, Japan). 384 Well Low Volume Plate Black Round-Bottom NBS was purchased from Corning (NY, USA). Other chemicals were purchased from FUJIFILM Wako Pure Chemical Corporation (Osaka, Japan) or Nacalai Tesque (Kyoto, Japan).

Synthesis of lipidated DNA: 200 μM of thiol-modified DNA oligonucleotides were treated with 10 mM TCEP (tris(2-carboxyethyl)phosphine) in 50 mM phosphate buffer (pH 8.0) for 30 min at room temperature and reacted overnight with 5 mM of DOPE-MAL containing 2% OG. The reaction mixture was purified by reverse-phase HPLC on a Cosmosil 5 C18-MS II column (4.6×150 mm, eluted with 0.1 M TEAA (triethylammonium acetate) buffer, pH 7.0, with a liner gradient over 10 min from 50 to 75% acetonitrile at a flow rate of 1.0 mL·min^{-1}) and characterized by MALDI-TOF mass spectrometry (AXIMA-LNR, Shimadzu, Kyoto, Japan) (HPA matrix). Lipidated ODN: m/z calculated 7637, observed 7640.

Preparation of the DNA scaffold: A solution (50 μL) containing M13 p7308 (10 nM) and mixture of staple DNA strands (50 nM) (Table S4) in a buffer (pH 8.0) containing 5 mM Tris-HCl, 1 mM EDTA, 14 mM $MgCl_2$ was incubated at 80 °C for 5 min, cooled down to 65 °C at 5 min/°C, incubated at 65 °C for 20 min, cooled down to 25 °C at 20 min/°C and then cooled down to 4 °C by using a thermal cycler (C1000 Thermal Cycler, BioRad).[33] The sample was purified by gel filtration on Ultrafree-MC–DV column to remove excess staple strands. The concentration of DNA scaffold was quantified by absorbance at 260 nm (Nanodrop, Thermo Fisher Scientific Inc.) using the determined extinction coefficient of DNA scaffold (1.17×10^8 M^{-1}cm^{-1}).

Preparation of liposome on DNA nanostructure: A solution containing 10 nM of DNA nanostructure, 360 nM of CF-modified DNA and 360 nM of A647 modified DNA, 720 nM of lipid-modified DNA and 1% OG in 5 mM Tris-HCl, 1 mM EDTA, 10 mM $MgCl_2$, 10 mM NaCl was incubated at 35 °C for 1 h. To form DNA scaffold templated liposomes, 25 μL of 5 mM DOPC (0.8% Rho-PE) was added to 50 μL of 10 nM lipid, CF and A647 labeled DNA scaffold to give a total volume of 75 μL and the solution was shaken for 30 min at room temperature. The solution was diluted with 75 μL of 5 mM Tris-HCl, 1 mM EDTA, 10 mM $MgCl_2$, 10 mM NaCl buffer containing 0.67% OG, and dialyzed overnight against 2 L of buffer. 190 μL of the recovered solution was mixed with 110 μL of 54% iodixanol in 1× hydration buffer and placed at the bottom of a centrifuge tube (11×34 mm, Beckman Coulter Inc.). Six additional layers of 0 to 18% iodixanol solution[29,32] in buffer were added to the centrifuge tube (Figure S6). The tube was spun in an MLA-130 rotor (Beckman Coulter Inc.) at 150,000 × g at 4 °C for 5 h, and the fractions (55 μL per fraction) were collected.

Agarose gel electrophoresis: Samples were run on a 1.5% agarose gel in 0.5 × TBE containing 10 mM $MgCl_2$ and 0.05% SDS at 50 V for 2 h in the cold storage chamber. The gel was visualized by using ChemiDoc™ MP (Bio-Rad) under the CF channel (λex = 475 nm, λem = 532 nm), Rho (λex = 532 nm, λem = 595 nm), or A647 channel (λex = 637 nm, λem = 700 nm).

AFM imaging: The purified DNA nanostructure was deposited on a mica surface (1.5 mm in diameter), adsorbed for 5 min at ambient temperature, and then washed three times with a buffer (pH 8.0) containing 40 mM Tris-HCl, 20 mM acetic acid, 14 mM $MgCl_2$. The sample was scanned in solution in tapping mode using a fast scanning AFM system (Nano Live Vision, RIBM Co. Ltd, Tsukuba, Japan) with a silicon nitride cantilever (Olympus BL-AC10DS-A2). At least three independent preparations of each sample were analyzed by AFM, and several images were taken from different areas of the mica surface.

TEM imaging: After removal of iodixanol through Amicon Ultra-0.5 mL Centrifugal Filters (30-kD NMWL) (2.5 μL), the sample was placed on a glow discharged TEM grid and incubated for 1 minute. The excess sample was then removed with filter paper and incubated with 2% uranyl acetate (2.5 μL) for 1 minute. Excess uranyl acetate was then removed with filter paper and another round of incubation with 2% uranyl acetate (2.5 μL) for 1 minute was performed. The samples were analyzed by using a TEM microscope (JEOL JEM-1400).

Fluorescence microscopy analysis of the pH change of the external buffer: The naked-WS containing ODN-tag1(biotin-ODN-tag1) (see Table S5), or lipo-WS and lipo-OmpF-WS containing biotin-modified lipid were loaded onto a μ-Slide I 0.2 Luer ibidi-Treat pretreated with biotinylated bovine serum albumin and neutravidin, adsorbed for 15 min at ambient temperature, and then washed three times with 50 mM phosphate buffer (pH 8.0). The fluorescence of the samples was observed using an IX-81 fluorescence microscope (Olympus) equipped with a 20× objective lens and a Xe lamp. Fluorescence images were captured with an electron multiplier CCD camera (Hamamatsu Photonics K.K.) at ambient temperature. After the fluorescence of CF, Rho, and A 647 were monitored sequentially (image: pH 8.0), the sample was washed with 50 mM phosphate buffer (pH 6.0) to change the pH of the external buffer. The fluorescence images of them were taken again at the same position (image: pH 6.0). Then the sample was washed again with 50 mM phosphate buffer (pH 8.0), and the fluorescence images were taken again at the same position (image: pH 8.0 again).

Fluorescence measurement: Fluorescence intensity of CF and A647 on DNA nanostructures (naked-WS) was measured at 25 °C using an Infinite 200 PRO microplate reader (TECAN, Austria, GmbH) with excitation at 480 nm and 620 nm in the 50 mM acetate (pH 5.5), PB (pH 6.0 to 6.5) or CHES (pH 8.0 to 9.0) buffer containing 12.5 mM $MgCl_2$, respectively. Fluorescence measurements were performed in 96-well plate.

Expression and purification of OmpF: OmpF expression was performed in LB medium supplemented with 50 mg/L kanamycin in shaking flasks. Cells were grown to an optical density at 600 nm of 0.6–0.8 at 37 °C and 250 rpm before protein expression was induced with isopropyl β-D-1-thiogalactopyranoside (IPTG) to a final concentration of 1 mM. Protein expression was allowed to proceed for 4 h at 37 °C and 250 rpm. Cells were harvested by centrifugation at 4000×g for 15 min at 4 °C. 20 mL of 10 mM Tris-HCl, pH 8.0 was added to resuspend the cell pellet. The solution was placed on ice

and treated with sonication. 1 mL of 20% SDS was added per 10 mL of cell suspension (2% SDS) and incubated for 1 h at 60 °C in a water bath with gentle stirring. The pellet was collected by ultracentrifugation at 15000 g for 90 min at 4 °C and the solution was discarded. The cell pellet was then rinsed several times with 20 mM phosphate buffer pH 8.0 to remove residual SDS. Then, 5 mL of 0.125% OG in phosphate buffer (pH 8.0) was added and the pellet was allowed to shake at 37 °C for 1 h to remove proteins from the pellet without solubilizing the porin. Again, the pellet was collected by ultracentrifugation at 4 °C for 40 min and the solution was discarded. Finally, the pellet was dissolved in 3% OG in phosphate buffer (pH 8.0) and shaken at 37 °C for 1 h. The solution was again ultracentrifuged at 40,000 rpm at 20 °C for 40 min, but this time the solution was retained and the pellet discarded (Figure S11).

Preparation and purification of lipo-OmpF-WS: Purified OmpF stored in phosphate buffer (pH 8.0) containing 3% OG, was mixed with purified lipo-WS (4 nM) to reach a final concentration of up to 1 μM (OG concentration is lower than 0.1%). The mixture was then incubated at 37 °C for 1 h to facilitate the insertion of OmpF from the external solution into the membrane. After immobilization of Lipo-OmpF-WS on the surface, the excess OmpF was washed three times with 50 mM phosphate buffer (pH 8.0).

Estimation of the number of OmpF per lipo-WS: The Lipo-OmpF-WS containing biotin-modified lipid was loaded onto a μ-Slide I 0.2 Luer ibidi-Treat pretreated with biotinylated bovine serum albumin and neutravidin. The slide was then adsorbed for 15 min at room temperature and washed three times to remove the excess OmpF. Lipo-OmpF-WS was then washed with 50 mM phosphate buffer (pH 8.0) containing 0.1% SDS to disrupt the liposome. The collected sample was concentrated three times using a 30 kDa Amicon Ultra tube with origami buffer. The concentration of DNA origami, which is equal to the concentration of liposome, was measured by NanoDrop and the average concentration was determined as shown in Table S3. The concentration of OmpF was measured by the band intensity of SDS-PAGE (Figure S12 and Table S3).

Fluorescence microscopy analysis for size-dependent permeability: The naked-WS containing biotin-modified staple strands, lipo-WS, and lipo-OmpF-WS containing biotin-modified lipid were loaded onto a μ-Slide I 0.2 Luer ibidi-Treat pretreated by biotinylated bovine serum albumin and neutravidin, adsorbed for 15 min at ambient temperature, and then washed three times with 50 mM phosphate buffer (pH 8.0). The fluorescence of the samples was observed using an IX-81 fluorescence microscope (Olympus) equipped with a 20×objective lens and a Xe lamp. Fluorescence images were captured with an electron multiplier CCD camera (Hamamatsu Photonics K.K.) at ambient temperature. After monitoring the fluorescence of A647, the sample was incubated with 10 nM EtBr/GelRed for 5 min. The sample was then washed again with 50 mM phosphate buffer (pH 8.0), and the fluorescence images were captured at the same position.

Fluorescence measurement for size-dependent permeability: The fluorescence intensity of EtBr and GelRed was measured at 25 °C using an Infinite 200 PRO microplate reader (TECAN, Austria, GmbH) with excitation at 490 nm and emission at 590 nm. 80 μL of WS, Lipo-WS or Lipo-OmpF-WS (1 nM) was added to a 96-well plate. Then, 10 nM EtBr or GelRed was added, and after 10 min 0.1% SDS was added to disrupt the liposome.

Acknowledgements

This work was supported by JSPS KAKENHI Grant No. 17H01213 and 23H02083(T.M.), 20H02860 and 22H05418 (E.N.) and by JST CREST Grant No. JPMJCR18H5 (T.M.), Japan. The TEM measurements in this work were supported by the Analysis and Development System for Advanced Materials (ADAM) of RISH, Kyoto University, as a collaborative program, or the Kyoto University Nano Technology Hub in the "Nanotechnology Platform Project" sponsored by the Ministry of Education, Culture, Sports, Science and Technology (MEXT), Japan.

Conflict of Interests

The authors have no conflicts of interest directly relevant to the content of this article.

Data Availability Statement

The data that support the findings of this study are available in the supplementary material of this article.

Keywords: compartment · DNA origami · liposome · membrane transporter · size exclusion transport

[1] J. R. Yates, A. Gilchrist, K. E. Howell, J. J. M. Bergeron, *Nat. Rev. Mol. Cell Biol.* **2005**, *6*, 702–714.
[2] J. W. Szostak, D. P. Bartel, P. L. Luisi, *Nature* **2001**, *409*, 387–390.
[3] E. Busto, R. C. Simon, N. Richter, W. Kroutil, *ACS Catal.* **2016**, *6*, 2393–2397.
[4] C. A. Denard, J. F. Hartwig, H. Zhao, *ACS Catal.* **2013**, *3*, 2856–2864.
[5] L. Zhang, K. Bellve, K. Fogarty, W. R. Kobertz, *Cell Chem. Biol.* **2016**, *23*, 1449–1457.
[6] R. J. R. W. Peters, I. Louzao, J. C. M. Van Hest, *Chem. Sci.* **2012**, *3*, 335–342.
[7] X. Zhang, M. Lomora, T. Einfalt, W. Meier, N. Klein, D. Schneider, C. G. Palivan, *Biomaterials* **2016**, *89*, 79–88.
[8] F. Ahmed, R. I. Pakunlu, G. Srinivas, A. Brannan, F. Bates, M. L. Klein, T. Minko, D. E. Discher, *Mol. Pharm.* **2006**, *3*, 340–350.
[9] T. Heinisch, K. Langowska, P. Tanner, J. L. Reymond, W. Meier, C. Palivan, T. R. Ward, *ChemCatChem* **2013**, *5*, 720–723.
[10] L. M. Ickenstein, P. Garidel, *Expert Opin. Drug Delivery* **2019**, *16*, 1205–1226.
[11] M. Brasch, R. M. Putri, M. V. De Ruiter, D. Luque, M. S. T. Koay, J. J. Castóncastón, J. J. L. M. Cornelissen, *J. Am. Chem. Soc.* **2017**, *139*, 1512–1519.
[12] Q. Hu, H. Li, L. Wang, H. Gu, C. Fan, *Chem. Rev.* **2019**, *119*, 6459–6506.
[13] F. Scaletti, J. Hardie, Y. W. Lee, D. C. Luther, M. Ray, V. M. Rotello, *Chem. Soc. Rev.* **2018**, *47*, 3421–3432.
[14] G. Sun, T. S. Chung, K. Jeyaseelan, A. Armugam, *Colloids Surf. B Biointerfaces* **2013**, *102*, 466–471.
[15] G. Ghale, A. G. Lanctôt, H. T. Kreissl, M. H. Jacob, H. Weingart, M. Winterhalter, W. M. Nau, *Angew. Chem. Int. Ed.* **2014**, *53*, 2762–2765.
[16] Y. M. Tu, W. Song, T. Ren, Y. xiao Shen, R. Chowdhury, P. Rajapaksha, T. E. Culp, L. Samineni, C. Lang, A. Thokkadam, D. Carson, Y. Dai, A. Mukthar, M. Zhang, A. Parshin, J. N. Sloand, S. H. Medina, M. Grzelakowski, D. Bhattacharya, W. A. Phillip, E. D. Gomez, R. J. Hickey, Y. Wei, M. Kumar, *Nat. Mater.* **2020**, *19*, 347–354.
[17] P. W. K. Rothemund, *Nature* **2006**, *440*, 297–302.
[18] C. Lin, R. Jungmann, A. M. Leifer, C. Li, D. Levner, G. M. Church, W. M. Shih, P. Yin, *Nat. Chem.* **2012**, *4*, 832–839.
[19] L. He, D. Q. Lu, H. Liang, S. Xie, C. Luo, M. Hu, L. Xu, X. Zhang, W. Tan, *ACS Nano* **2017**, *11*, 4060–4066.

[20] X. Shen, C. Song, J. Wang, D. Shi, Z. Wang, N. Liu, B. Ding, *J. Am. Chem. Soc.* **2012**, *134*, 146–149.
[21] A. Kuzyk, R. Schreiber, Z. Fan, G. Pardatscher, E.-M. Roller, A. Högele, F. C. Simmel, A. O. Govorov, T. Liedl, *Nature* **2012**, *483*, 311–314.
[22] J. Fu, M. Liu, Y. Liu, N. W. Woodbury, H. Yan, *J. Am. Chem. Soc.* **2012**, *134*, 5516–5519.
[23] O. I. Wilner, Y. Weizmann, R. Gill, O. Lioubashevski, R. Freeman, I. Willner, *Nat. Nanotechnol.* **2009**, *4*, 249–254.
[24] M. Liu, J. Fu, X. Qi, S. Wootten, N. W. Woodbury, Y. Liu, H. Yan, *ChemBioChem* **2016**, *17*, 1097–1101.
[25] T. M. Nguyen, E. Nakata, M. Saimura, H. Dinh, T. Morii, *J. Am. Chem. Soc.* **2017**, *139*, 8487–8496.
[26] T. A. Ngo, E. Nakata, M. Saimura, T. Morii, *J. Am. Chem. Soc.* **2016**, *138*, 3012–3021.
[27] G. Ke, M. Liu, S. Jiang, X. Qi, Y. R. Yang, S. Wootten, F. Zhang, Z. Zhu, Y. Liu, C. J. Yang, H. Yan, *Angew. Chem. Int. Ed.* **2016**, *55*, 7483–7486.
[28] Y. Dong, S. Chen, S. Zhang, J. Sodroski, Z. Yang, D. Liu, Y. Mao, *Angew. Chem. Int. Ed.* **2018**, *57*, 2072–2076.
[29] Y. Yang, J. Wang, H. Shigematsu, W. Xu, W. M. Shih, J. E. Rothman, C. Lin, *Nat. Chem.* **2016**, *8*, 476–483.
[30] Z. Zhang, Y. Yang, F. Pincet, M. C. Llaguno, C. Lin, *Nat. Chem.* **2017**, *9*, 653–659.
[31] X. Bian, Z. Zhang, Q. Xiong, P. De Camilli, C. Lin, *Nat. Chem. Biol.* **2019**, *15*, 830–837.
[32] H. Konishi, E. Nakata, F. Komatsubara, T. Morii, *Molecules* **2023**, *28*, 911.
[33] S. D. Perrault, W. M. Shih, *ACS Nano* **2014**, *8*, 5132–5140.
[34] P. S. Phale, T. Schirmer, A. Prilipov, K. L. Lou, A. Hardmeyer, J. P. Rosenbusch, *Proc. Nat. Acad. Sci.* **1997**, *94*, 6741–6745.
[35] J. Han, K. Burgess, *Chem. Rev.* **2010**, *110*, 2709–2728.
[36] Y. H. M. Chan, B. Van Lengerich, S. G. Boxer, *Proc. Nat. Acad. Sci.* **2009**, *106*, 979–984.
[37] M. Ollivon, S. Lesieur, C. Grabielle-Madelmont, M. Paternostre, *Biochim. Biophys. Acta Biomembr.* **2000**, *1508*, 34–50.
[38] K. W. Dunn, M. M. Kamocka, J. H. McDonald, *Am. J. Physiol. Cell Physiol.* **2011**, *300*, 723–742.
[39] E. Nakata, H. Hirose, K. Gerelbaatar, J. V. V. Arafiles, Z. Zhang, S. Futaki, T. Morii, *Chem. Sci.* **2021**, *12*, 8231.
[40] R. Koebnik, K. P. Locher, P. Van Gelder, *Mol. Microbiol.* **2000**, *37*, 239–253.
[41] E. Nakata, F. F. Liew, C. Uwatoko, S. Kiyonaka, Y. Mori, Y. Katsuda, M. Endo, H. Sugiyama, T. Morii, *Angew. Chem. Int. Ed.* **2012**, *51*, 2421–2424.
[42] E. Nakata, H. Dinh, T. A. Ngo, M. Saimura, T. Morii, *Chem. Commun.* **2014**, *51*, 1016–1019.
[43] T. A. Ngo, E. Nakata, M. Saimura, T. Morii, *J. Am. Chem. Soc.* **2016**, *138*, 3012–3021.

Manuscript received: July 1, 2023
Accepted manuscript online: September 5, 2023
Version of record online: October 17, 2023